JOURNAL OF MATERIALS SCIENCE 32 (1997) 1287–1295

Mode II delamination failure mechanisms of polymer matrix composites

SHAW MING LEE
Hexcel Corporation, 5115 E. LaPalma Avenue, Anaheim, CA 92807 USA

The failure process of mode II delamination fracture is studied on the basis of the microscopic matrix failure modes (microcracks and hackles) as well as fracture mechanics principles. The crack tip matrix stresses leading to delamination is analysed by examining an adhesive bond with a crack analogous to a delamination crack in the resin layer of a composite. Such crack tip stresses induce matrix microcracks involving two major events: (a) single microcrack initiation and (b) development of multiple microcracks with regular spacing. The microcrack initiation shear stress τ^* is found by the use of fracture mechanics to be related to certain resin properties (shear modulus G and mode I fracture toughness G_{IC}) and microcrack length of the order of the resin layer thickness t (related to resin content). The more or less regular microcrack spacing S deduced from shear lag considerations can be related to resin properties G_{IC}, G, τ_y (resin yield strength) and t. The multiple microcracks reduce the effective resin modulus and strongly affect the subsequent microcrack coalescence process. As a result of the detailed analysis of the failure process, mode II laminate fracture toughness G_{IIC} can be quantitatively expressed as a function of resin G_{IC} and (τ_y^2/G). The failure process modelled is used to interpret the mode II delamination behaviour of several carbon/epoxy systems studied here and that reported in the literature. This study reveals the critical importance of resin fracture (G_{IC} related) and deformation (yielding) mechanisms in controlling mode II delamination resistance of laminated composites.

1. Introduction

Mode II delamination in laminates is a major matrix-controlled failure mode induced by out-of-plane shear stresses frequently encountered in composite structures. As a fundamental failure mode, mode II delamination strongly influences a wide range of structural behaviour under out-of-plane loading, especially that due to surface loading such as impact. From the standpoint of the failure mechanisms involved, the deformation and fracture behaviour of the resin between fibres at the microscopic level must critically control the macroscopic composite behaviour related to this failure mode. Although the morphology of mode II crack growth can be qualitatively related to the driving stress state, a quantitative description of the failure process involved is still lacking. As a result, the exact matrix material variables governing this failure mode have not been clearly identified.

Mode II delamination of laminates is often typified by the pronounced microscopic "hackle" marking [1–5] of the resin matrices on the fracture surfaces. The occurrence of such marking can be attributed to the tendency of the resin to fail in mode I caused by local maximum principal stresses that are oriented at an angle to the crack plane. In other words, mode II failure at the macroscopic level largely grows in a plane between fibres as a result of the shear stresses in that plane. At the microscopic level, the crack tends to deviate from the plane in favour of the maximum principal tensile stresses. However, because of the constraints of fibres such crack deviation was limited to the matrix between fibres but multiplied along the entire crack path to form the hackle pattern [1–5]. The mode II delamination behaviour therefore must be critically determined by the failure process resulting in such a hackle pattern.

In this paper, a mechanistic model constructed to account for the mode II crack growth process is reported. In this model the crack tip stress distribution in the resin layer is derived from an adhesive joint analogy representing the matrix-controlled behaviour of laminated composites. The microcracking event in relation to the resin properties is obtained on the basis of fracture mechanics principles. The coalescence of the microcracks leading to the macroscopic crack propagation is found to be determined by the crack tip stress level and microcrack density. A parametric representation of laminate mode II fracture toughness, G_{IIC}, is then reached in terms of the relevant resin properties. The theory is applied to interpret the mode II fracture behaviour of several carbon fibre/epoxy systems based on their matrix resin properties.

0022–2461

2. Mode II failure model

The mode II delamination failure process analysed here focuses on the microscopic crack tip damage growth in the thin resin layer along the crack path between the fibres in the composite. The nature of the mode II delamination crack tip stresses in the resin matrix is first determined by analysing the local stress distribution in a typical mode II laminate test configuration. The crack tip damage in the form of microcracks, reflecting the hackles often observed on the mode II fracture surfaces, is then modelled on the basis of the derived crack tip stresses as well as fracture mechanics principles. The coalescence of these microcracks results in macroscopic crack propagation and is related to the macroscopic composite mode II fracture toughness or strain energy release rate G_{IIC}. Since the crack tip stresses, microcracks formation and their coalescence are all dependent on certain resin deformation and fracture properties, laminate G_{IIC} can be expressed in parametric form as a function of these resin properties. From this mode II failure model, the mode II delamination failure mechanisms and the controlling resin behaviour are identified. It should be pointed out that the failure model is established here with certain simplifying assumptions based on well observed physical details related to mode II delamination.

To analyse mode II delamination failure, the problem focused on here is the well established end notched flexure (ENF) method [6–8] in which a unidirectional specimen (Fig. 1a) with a crack of length a is subject to simple three point loading. The analysis would allow the microscopic failure process to be directly related to the macroscopically measured fracture parameter G_{IIC}. The solution obtained here is, however, by no means limited to the ENF specimen and should be applicable to general mode II failure configurations. To simplify the analysis, the composite ENF specimen is conceptually replaced with an adhesive joint with the same geometry (Fig. 1b). The adhesive represents the thin resin layer between the fibres and a crack is located at the mid-plane of the resin. The adherends, on the other hand, are homogeneous with elastic properties identical to those of the composite material and are much stiffer than the adhesive. Such an analogy between composite and adhesive joint is similar to that used in analysing mode I delamination [9–11]. The approach allows the complicated 3-dimensional composite problem to be analysed in a 2-dimensional manner allowing critical insights of the nature of crack tip stress distribution.

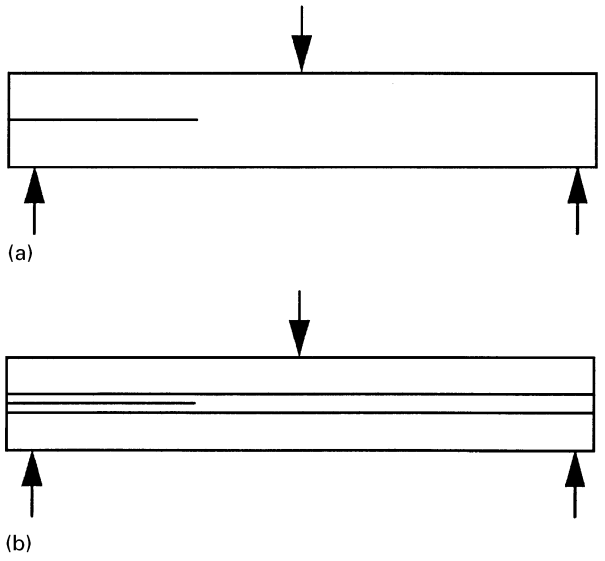

Figure 1 (a) A delamination crack in a unidirectional laminate ENF specimen is modelled as (b) a crack in an adhesive joint with its adherends having the same properties as the laminate.

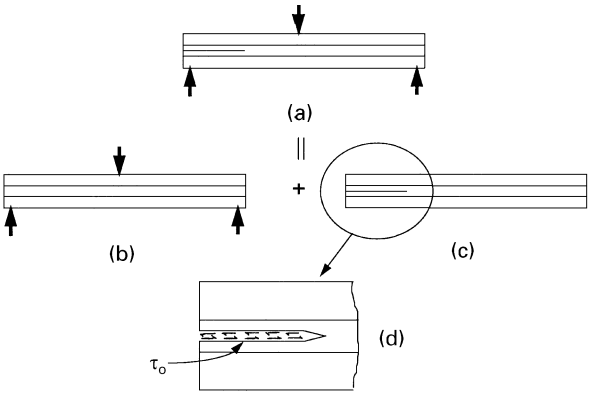

Figure 2 The stress distribution in (a) an adhesive joint ENF specimen subject to 3 point loading is equal to the superposition of (b) that in an equivalent specimen without a crack but under the same loading condition and (b) that in the ENF specimen with only shear traction τ_0 on the crack surfaces. The detailed loading condition for case (c) is illustrated in (d).

2.1. Crack tip stress distribution

The detailed crack tip stress field induced in the thin resin layer along the crack path is derived below. For the ENF specimen analysed, the case of the adhesive without microcracks ahead of the macroscopic crack is addressed at the moment but the solution found can be applied to the case with microcracks as will be discussed later. The adhesive joint ENF specimen under a centre load P (Fig. 2a) is equivalent to the superposition of the specimen without a crack under load P (Fig. 2b) and the specimen with a crack subject to uniform applied shear stress τ_0 on the crack surfaces (Fig. 2c). The shear stress τ_0 has the same magnitude, but in the opposite direction, as that induced in the mid-plane of case in Fig. 2b, thus satisfying the stress free condition in the crack after superposition. τ_0 can be easily found to be

$$\tau_0 = \frac{3P}{8Bh} \tag{1}$$

where h is the half specimen thickness and B the specimen width. The mode II crack tip stress distribution can, therefore, be found from the case (Fig. 2c) with shear traction on the crack surfaces.

The ENF specimen with crack surfaces subject to shear stress can be treated as a beam deformation problem of the upper and lower adherends. Each adherend is deformed by the shear stresses along the

adhesive/adherend interfaces. The existing crack is assumed to be in the mid-plane of the resin layer of thickness t. This mid-plane crack assumption is, however, not critical for the current analysis as will be discussed later. For the x–y coordinate system with its origin at the crack tip (Fig. 3), a uniform stress τ_0 is applied to the adherends for $-a \leqslant x < 0$. For $x \geqslant 0$, shear stress $\tau(x)$ and x-direction displacement $u(x)$ are induced at the interfaces between the adherend and the adhesive ($y = t/2$ and $-t/2$). Because of the antisymmetric nature of loading exerted upon the upper and lower adherends, $\tau(x)$ and $u(x)$ of the two adherends are equal in magnitude but different in sign at any given x. Therefore, only one adherend, the upper one, needs to be treated to solve for τ and u. As the u profiles of the adherends are antisymmetric about the x axis, the resin must have zero displacement along this axis.

It is assumed that the shear stress τ_{xy} is only a function of x and independent of y in the thin resin layer. This assumption is reasonable as the resin layer thickness t is orders of magnitude smaller than the ENF beam thickness. It however ignores the singular nature of the crack tip stresses when x is very small and τ should theoretically vary with y. Such stress singularity is actually not all that critical for the mode II delamination growth involving matrix microcracks reflected by the unique hackle pattern of fracture surface morphology. As these microcracks are isolated from each other before coalescence, they must be induced by stresses at a certain distance away from the exact crack tip. (Otherwise, the stress singularity would always drive the crack to grow into a single continuous crack instead of multiple microcracks.) In reality, in response to the shear loading, an introduced crack itself would most likely grow at an angle (45°) to terminate at the adhesive/adherend interface, thus resulting in maximum shear stresses at a distance away from the terminated crack tip. Therefore, the assumption of τ independent of y is accurate except for very small x (very close to the crack tip) where the stress state does not directly control the microcrack formation process as the experimentally observed hackle marking indicates. Also because the stresses relevant to inducing microcracks are non-singular in nature, the mid-plane crack assumption mentioned before is not critical for the model.

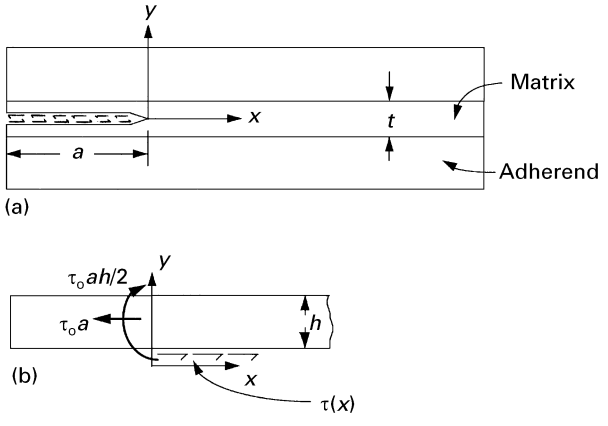

Figure 3 (a) Crack tip coordinate system (x–y) in relation to the adherends; and (b) the free-body diagram for a portion ($x \geqslant 0$) of the upper adherend subject to crack surface traction $\tau(x)$.

The resin shear stress $\tau = \tau_{xy}$ assumed to be independent of y must be of a constant value through the resin layer thickness as well as at the adhesive/adherend interfaces at any x ahead of the crack tip ($x > 0$). As a result, the shear strain γ in the resin should also be independent of y and can be expressed in terms of u as

$$\gamma = \frac{2u}{t} \tag{2}$$

where t is the thickness of the adhesive layer. The shear stress τ can be related to γ and u by

$$\tau = -G\gamma = -2Gu/t \tag{3}$$

where G is the resin shear modulus. The negative sign in Equation 3 is necessary to relate τ applied to the adherend to γ induced in the adhesive.

A free body diagram of the adherend for $x > 0$ is shown in Fig. 3b. The stress along the adhesive/adherend boundary is induced by axial loading and bending of the beam. At any $x > 0$, the axial load T per unit width in the mid-plane of the adherend ($y = h/2$)

$$T = \tau_0 a - \int_0^x \tau \, d\chi \tag{4}$$

The corresponding strain ε_T at $y = t/2$ caused by T is

$$\varepsilon_T = T/E_L h = \left(\tau_0 a - \int_0^x \tau \, d\chi\right) \Big/ E_L h \tag{5}$$

where E_L is the longitude modulus (x-direction) of the adherend or the composite. The bending moment M per unit width in the adherend ($y = h/2$) at x is

$$M = \left(\tau_0 ah - h\int_0^x \tau \, d\chi\right) \Big/ 2 \tag{6}$$

The strain ε_b along $y = t/2$ due to M is

$$\varepsilon_b = M(h/2)/E_L I = 3\left(\tau_0 a - \int_0^x \tau \, d\chi\right) \Big/ E_L h \tag{7}$$

where $I = h^3/12$ is the moment of inertia per unit width. The total strain ε at $y = t/2$ is

$$\varepsilon = \varepsilon_T + \varepsilon_b = 4\left(\tau_0 a - \int_0^x \tau \, d\chi\right) \Big/ E_L h \tag{8}$$

Differentiation of Equation 3 with respective to x yields

$$\frac{d\tau}{dx} = -\left(\frac{2G}{t}\right)\left(\frac{du}{dx}\right) = -\frac{2G\varepsilon}{t} = -\frac{8G(\tau_0 a - \int_0^x \tau \, d\chi)}{E_L th} \tag{9}$$

Equation 9 can be further differentiated to result in

$$\frac{d^2\tau}{dx^2} = \frac{8G\tau}{E_L th} \tag{10}$$

The solution of the above differential equation is obtained by considering $\tau = 0$ as x:

$$\tau = \tau^* \exp(-kx) \tag{11}$$

where $k = (8G/E_L th)^{1/2}$ and τ^* is a constant. To solve for τ^*, the equilibrium between the applied load versus the induced reacting load is considered. This leads to

$$\tau_0 a = \int_0^x \tau \, dx = \tau^*/k \tag{12}$$

by using τ given in Equation 11. τ^* is, therefore, simply

$$\tau^* = \tau_0 ak \tag{13}$$

The crack tip shear stress τ can therefore be found from Equations 11 and 13 to be

$$\tau = \tau_0 ak \exp(-kx) \tag{14}$$

It is interesting to note that the exponential dependence of τ on x implies stress concentration extending to a distance of the order of $1/k$. For a typical ENF specimen, $G = 1.4$ GPa psi (resin), $E_L = 14$ GPa, $h = 15$ mm, and $t = 0.025$ mm. k is found to be $1.46\ \text{mm}^{-1}$. The heavy crack tip stress concentration region is estimated to be of the order of 0.7 mm ($\sim 1/k$).

The true crack tip shear stress is the superposition of the stress τ induced in Fig. 2c (Equation 14) and τ_0 induced in Fig. 2b (Equation 1), i.e., $\tau_0 + \tau = \tau_0 (1 + ak \exp(-kx))$. However, as $ak \gg 1$, close to the crack tip τ is obviously much larger than τ_0 and $\tau = \tau_0 ak \exp(-kx)$ likely dominates the crack tip stress field. Therefore, τ expressed in Equation 14 will be used to represent the crack tip stress for further derivation of the failure process involved.

2.2. Microcrack formation

The multiple microcracks induced in the resin layer along the crack path have been well recognized to result in "hackle" marking on the fracture surfaces. Such marking in composites is more pronounced for relatively brittle matrices than for ductile or tough ones. The microcracks are obviously induced by the maximum principle stress in the shear dominant stress field at the crack tip. They are also most likely initiated independently in the crack tip "process zone" [1–5]. Further loading leads to the coalescence of the microcracks and thus macroscopic crack extension.

The microcrack formation process for mode II delamination is studied by examining the two major events involved in the failure process: (1) the creation of an isolated microcrack and (2) the development of multiple microcracks with almost regular spacing. The case of a single microcrack can be treated as a fracture nucleation and growth problem. The subject of crack spacing, on the other hand, can be considered in a manner similar to shear lag theory [12–14] to determine the distance of stress field affected by a microcrack.

2.2.1. Single microcrack growth

A single microcrack is considered to grow in the resin layer constrained by adherends representing the composite (Fig. 4) following the adhesive joint analogy discussed previously. The single crack is assumed to be induced by a locally uniform maximum crack tip shear stress τ^*. This crack aligned at a 45° direction with respective to the plane of the resin layer is perpendicular to the maximum principal stress associated with the pure shear stress field. It should be pointed out that the crack tip shear stress $\tau = \tau^* \exp(-kx)$ (Equation 14) strictly speaking is a function of x. However, over the distance of the microcrack spacing (of the order of t) the theoretical shear stress variation is small as is shown in Fig. 4 (for example, by considering $t = 0.025$ mm and $k = 1.46\ \text{mm}^{-1}$ discussed previously).

Another assumption implied here is that the maximum shear stress in the resin is located at the single microcrack focused on here. This point is physically reasonable as the microcrack should occur at the maximum shear stress. The reason for the microcrack in isolated form is that the stress profile described by Equation 14 is not accurate for small x. Actually, through stress transfer at the resin/adherend interface, the stresses in the resin layer relevant to the cracking process likely increase from a low value at the existing macroscopic crack (or microcrack) to reach a maximum value close to τ^* for crack formation as is shown in Fig. 4. Once such a microcrack is developed the local stress will be redistributed to shift the maximum shear stress ahead by a distance to induce the next crack. Such a distance between microcracks is related to crack spacing to be discussed later.

The formation of a single microcrack is examined here based on the energy principles of fracture mechanics. The microcrack causes strain energy to be released from the originally uniform shear stress state. Such a released energy, on the other hand, must be consumed and thus balanced by the energy associated with creating the new crack surface. The microcrack is assumed to be of crack length a which can be related to the resin thickness t by

$$a = \alpha t \tag{15}$$

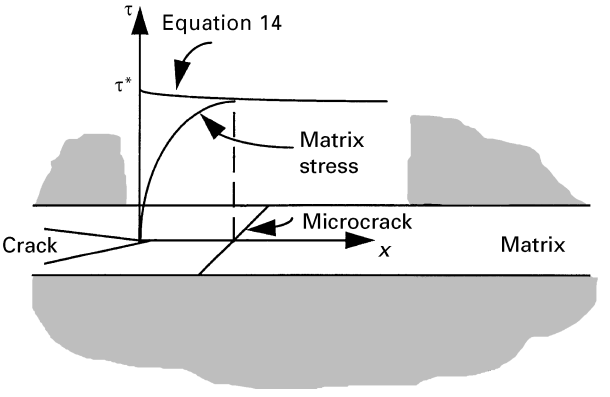

Figure 4 Shear stress in the matrix layer reaches a maximum value at a distance ahead of an existing crack to cause microcracking.

where $0 < \alpha < (2)^{1/2}$. Although α is close to $(2)^{1/2}t$ for a fully extended crack, the value of α is not specified at the moment for generality. Without having the exact stress distribution for the case of a crack in a constrained resin layer shown in Fig. 4, the energy release U_1 caused by the crack can be estimated in an approximate manner. The deformation caused by the shear stress τ^* is assumed to be linear elastic without the presence of gross matrix plastic deformation to suppress matrix fracture. The presence of the crack can be assumed to release the strain energy of original density $\tau^{*2}/2G$ in a volume of the order of βa^2 to result in:

$$U_1 = (\tau^{*2}/2G)\beta a^2 = (\tau^{*2}/2G)\beta\alpha^2 t^2 \qquad (16)$$

where β is a constant which can be assumed to be smaller than but of the order of $\pi/2$ for the case of a crack in an infinite medium [15]. The energy U_2 consumed for creating the microcrack surface can be related to the mode I critical strain energy release rate G_{IC} of the matrix, i.e.,

$$U_2 = aG_{IC} = \alpha t\ G_{IC} \qquad (17)$$

As the energy balance requires that $U_1 = U_2$, equating and rearranging Equations 16 and 17 results in

$$\tau^* = [2GG_{IC}/\alpha\beta t]^{1/2} \qquad (18)$$

Equation 18 indicates that the formation of a microcrack in the localized crack tip damage zone is controlled by resin stiffness and fracture parameters (G and G_{IC}) as well as resin layer thickness (related to resin content). A rough estimate using Equation 18 based on $G = 1.4$ GPa, $G_{IC} = 0.18\ \text{kJ m}^{-2}$, $t = 0.025$ mm, $\alpha = 1$, and $\beta = 2$ gives a τ^* value of 100 MPa. Since τ^* is the local resin stress, there is a possibility that resin plastic deformation may occur first before the microcrack can be induced. Equation 18 therefore represents the condition of τ^* being smaller than the resin shear yield stress τ_y (i.e., $\tau^* < \tau_y$). For composite systems showing hackle patterns of fracture surface morphology, this indeed is the most likely case. If the theoretical τ^* value of the material according to Equation 18 is larger than resin τ_y, the crack tip stress concentration would result in resin yielding to suppress microcracking. This is the possible case for composite systems with relatively high G_{IC} and low τ_y such as PEEK or other thermoplastics-based composites [5].

2.2.2. Multiple microcracks and crack spacing

As previously discussed, the occurrence of a single crack would result in re-arrangement of the original stress field around this crack. The resin shear stress τ_{xy} (in the middle of the resin layer not at the resin/adherend interface) should now vanish at the very location of the microcrack ($x = 0$, $y = 0$) and gradually builds up to reach a maximum stress level $\tau^{*\prime}$ at a distance S away from the crack as shown in Fig. 5. The new location of the maximum shear stress will eventually become the new site for the next microcrack. However, at the instance of microcrack onset without increasing the applied external load, this new maximum shear stress $\tau^{*\prime}$ is slightly lower than τ^* needed for crack formation. To further induce a new microcrack ahead of the existing one, the external load has to be increased by only an incremental amount to raise the maximum shear stress from $\tau^{*\prime}$ to τ^*. This failure process would then repeat itself as the applied load is incrementally increased to result in multiple microcracks along the crack path.

The mean crack spacing S being related to the shifting of the maximum shear stress due to the presence of a single crack can be modelled in a manner similar to the shear lag theory [12–14]. A simple case of a 45° single microcrack in an adhesive joint subject to remote uniform shear stress τ^* (Fig. 6a) can give important insights into the size of the stress field affected by such a microcrack.

Although the ideal uniform remote stress field is not exactly the same as the true one varying with x, the distance over which the stress distribution affected by the crack should be similar between the two cases. Besides, the stress field of interest should vary slowly within a distance of the order of the resin thickness affected by the crack as previously discussed. The ideal case (a) in Fig. 6a is a superposition of two cases: (b) the adhesive joint without a crack subject to uniform shear stress τ (Fig. 6b) and (c) the adhesive joint with a crack subject to crack surface normal stress σ^* ($= \tau^*$) but no remote shear stress (Fig. 6c). Note that the normal stress σ^* in case (c) is simply the maximum principle stress that induces the single crack in the first place. Since there is no stress non-uniformity in case (b), the stress field perturbed by a single microcrack can be found by simply examining case (c). For all the following analyses, all forces mentioned imply being forces per unit width in the z direction perpendicular to the x–y plane.

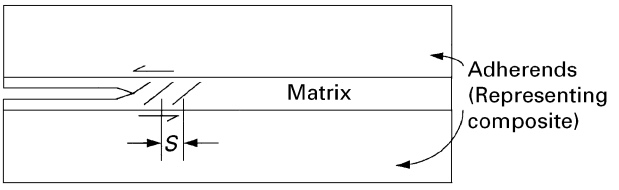

Figure 5 Multiple microcracks are induced in front of the mode II delamination crack tip with regular crack spacing S.

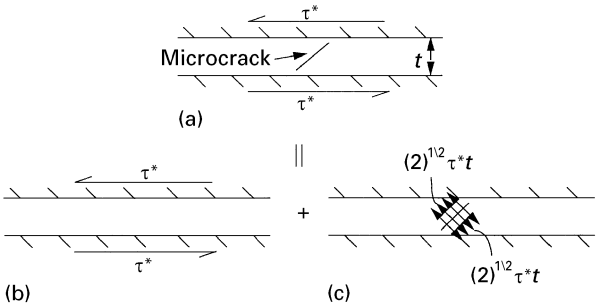

Figure 6 (a) A matrix microcrack in an adhesive joint subject to uniform shear stress τ^* is the superposition of (b) the same adhesive joint without a crack subject to the same shear stress and (c) the matrix microcrack surfaces subject to only normal surface traction $\tau^* t$.

The simple qualitative trend of such a distribution can be deduced without solving for the exact stress distribution around a single microcrack in the resin layer. The load transfer between the resin layer and the adherend for case (c) as a result of the applied load σ^* can be first examined for only a half ($x \geqslant 0$) of the resin layer. The total applied normal force to the microcrack at $x = 0$ is $(2)^{1/2}\tau^* t$ which has an x force component equal to $\tau^* t$. Such a force is balanced by the shear stress distribution τ', assumed with a similar profile, at the resin/adherend interfaces ($y = \pm t/2$). By shear-lag consideration [12–14], such a shear stress is decaying exponentially away from the microcrack function and can be represented by (Fig. 7a)

$$\tau'(x + t/2) = A_1 \exp(-\phi x) \quad \text{for } y = t/2 \tag{19}$$

$$\tau'(x - t/2) = -A_1 \exp(-\phi x) \quad \text{for } y = -t/2 \tag{20}$$

where A_1 and ϕ are constants dependent on the applied load and material properties involved. Such a stress distribution after superposition with a pure shear stress of τ^* (case (b)) leads to the shear stress τ at the resin/adherend interface for case (a) shown in Fig. 7b:

$$\tau(x + t/2) = \tau^* + A_1 \exp(-\phi x) \quad \text{for } y = t/2 \tag{21}$$

$$\tau(x - t/2) = \tau^* - A_1 \exp(-\phi x) \quad \text{for } y = -t/2 \tag{22}$$

By considering the site of the next 45° resin microcrack being located at $x = S$ where $\tau' \to 0$ for case (c), shear stresses τ for case (a) at two interfaces ($y = \pm t/2$) and in the resin should all reach τ^* to induce a new microcrack there. Physically, it means that when $\tau' \to 0$ at the resin/adherend interface, the stresses in the resin layer relevant to microcracking will be fully developed to reach the maximum values as shown in Fig. 4.

All the above discussion so far has assumed linear elastic material behaviour. In reality, stress concentration at the upper interface ($\tau = \tau^* + \tau'$) at least for small x can reach such a high level that the resin yield strength τ_y can be exceeded. It should be pointed out that plastic deformation induced in this case is likely localized close to the interface ($y = t/2$) and the resin layer can develop a more or less uniform shear stress τ^* at $x = S$ for microcrack formation. This is different from the case of $\tau^* > \tau_y$ discussed before in the single crack formation section where gross plastic deformation would occur thus preventing the resin layer ever achieving the shear stress of τ^* for microcracking.

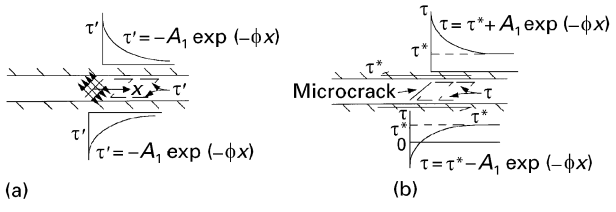

Figure 7 Resin/adherend interface shear stress distributions for (a) the microcrack in an adhesive joint subject to crack surface traction $\tau^* t$ and for (b) that subject to remote shear stress τ^*.

The effect of resin yielding on the crack spacing S due to the stress profile τ can be assessed by examining the three simple conditions: (i) $\tau^* > \tau_y$ (ii) $\tau^* < \tau_y$ and (iii) $\tau^* \ll \tau_y$ as is shown in Fig. 8. For condition (i), easy plastic deformation will dominate the resin layer without inducing microcrack to result in $S \to \infty$. Ductile tearing of the resin is the likely failure mode in this case. For condition (ii), significant plastic deformation is induced in a region with a distance of the order of S which can be qualitatively related to τ^* and τ_y by

$$\tau_y S \propto \tau^* t \tag{23}$$

As a first order approximation, the above equation physically means that a shear load caused by a yield strength τ_y and zone size S is proportional to the tensile load component $\tau^* t$ in the resin layer related to microcracking. For $\tau^* \ll \tau_y$ of condition (iii), plastic deformation may be highly localized close to the microcrack or completely suppressed. The corresponding crack spacing S is probably proportional to the resin layer thickness, i.e., $S \propto t$.

For composites mode II failure with obvious hackle marking related to microcracks, condition (i) would not be valid. Composites with matrices such as epoxies having typical properties of $\tau_y = 120$ MPa and $\tau^* = 100$ MPa (estimated previously in section 2.2.1) would be more accurately described by condition (ii) than by condition (iii). (Condition (iii) may be more valid for very brittle matrices such as ceramics.) Therefore, crack spacing, defined by Equation 23, can be reduced by considering Equation 18 to reach

$$S \propto (tG_{IC}G/\tau_y^2)^{1/2} \tag{24}$$

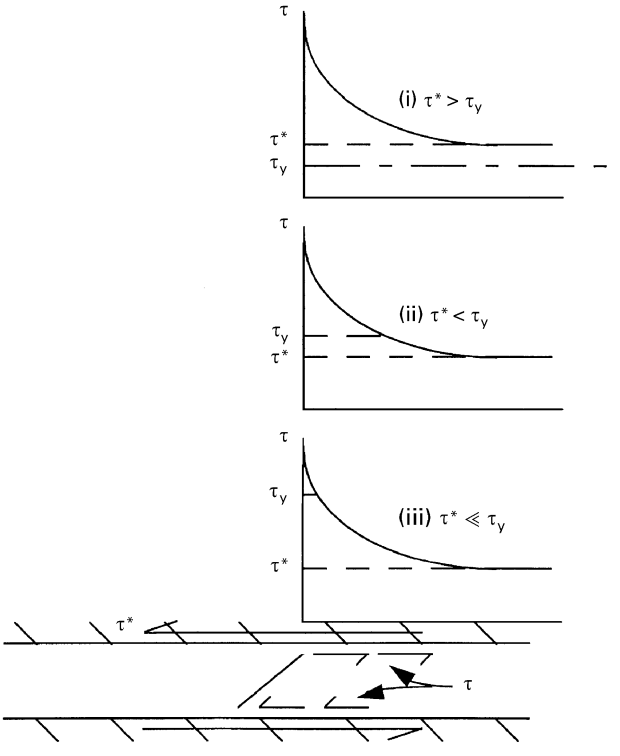

Figure 8 Shear stresses at resin/adherend interface ahead of a microcrack in relation to matrix yield strength τ_y.

2.3. Microcrack coalescence

The microcracks with spacing S (e.g., Equation 24) have two major effects on the mode II failure. Firstly, these cracks reduce the effective modulus of the resin in the zone with such microcracks. This will affect the stress distribution in the zone containing such cracks. Secondly, the spacing between cracks affects the local stress required to cause crack coalescence.

The elastic modulus, tensile or shear, is known to decrease with increasing presence of cracks in the material. The crack spacing S and resin thickness t would affect the resin layer shear deformation behaviour. The effective shear modulus G^* of the resin layer (in response to shear loading at the resin/adherend interface) as a function of S/t can be qualitatively plotted in Fig. 9 where G^* increases with S/t and asymptotically approaches G for a resin layer with a large S/t value. The high concentration of microcracks observed on mode II fracture surfaces would appear to drastically affect the elastic response of the resin layer. Therefore, the rising trend of G^* versus S/t in Fig. 9 is most likely the case involved. An approximate mathematical representation of G^* in terms of S/t for this case can be expressed as

$$G^* \alpha\, G(S/t)^{\mathrm{m}} \tag{25}$$

where $1 > m > 0$ is a constant of which the numerical range is deduced from the shape of the G^*–S/t curve.

The crack tip stress distribution in the region with multiple microcracks is obviously highly non-uniform. However, effective shear stress averaged over the crack spacing can at least be assessed from the reduced effective shear modulus by replacing G with G^* in Equations 3–14 related to crack tip stress distribution. The maximum effective crack tip stress τ_c so defined ($x = 0$) can be found from Equation 14 to be

$$\tau_c = \tau_0 a(8G^*/E_L th)^{1/2} \tag{26}$$

By substituting Equation 25 and τ_0 given in Equation 1 into Equation 26, τ_c becomes

$$\tau_c \propto (3Pa/8Bh)\,(8GS^{\mathrm{m}}/E_L t^{\mathrm{m}+1} h)^{1/2} \tag{27}$$

It is assumed that when τ_c reaches the critical level to cause microcrack coalescence the macroscopic crack advances. The microcracks essentially have to grow from their isolated form (Fig. 10a) to become interconnected with a crack of length S bridging between two microcracks (Fig. 10b). This process is likely to propagate from the very macroscopic crack tip along the crack path. The value of τ_c for such crack coalescence can be deduced from fracture mechanics principles in a way similar to that for reaching τ^* in Equation 18. The microcrack coalescence process of inducing a crack of length S connecting between two neighbouring microcracks is assumed to occur when the strain energy released is balanced by the fracture energy for creating connecting cracks. The strain energy released by such a crack is proportional to $(\tau_c^2/2G)S^2$ (similar to Equation 17) and the fracture energy consumed is equal to SG_{IC}. Equating these energies leads to:

$$\tau_c \propto (GG_{IC}/S)^{1/2} \tag{28}$$

which is similar to Equation 18. Note that G instead of G^* is used in the $(\tau_c^2/2G)$ term above to represent the local strain energy density around the new crack of length S. Whereas G^*, on the other hand, is an effective modulus reflecting the macroscopic behaviour of the resin volume bounded by the microcracks spacing S and the resin layer thickness t. The connecting crack between the microcracks is not expected to entirely relieve the stresses in this resin volume at least at the onset stage of such a crack. This can be evidenced by the fact that cracks can be induced, for instance, at the bottom of the resin layer after the connecting cracks are fully developed at the top as shown in references [16, 17] and depicted in Fig. 11.

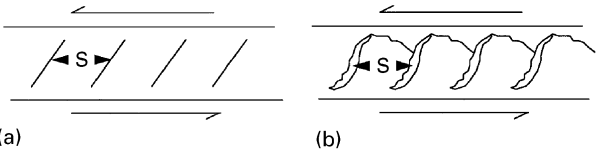

Figure 10 The multiple microcracks change from (a) isolated form to (b) coalescence form as the shear stress builds up.

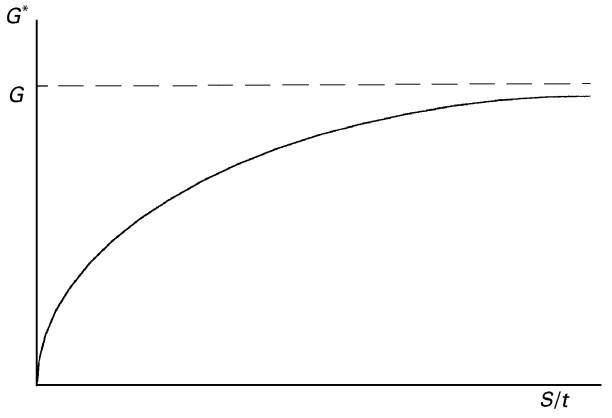

Figure 9 Effective shear modulus G^* of the matrix resin layer as a function of crack spacing S and resin layer thickness t.

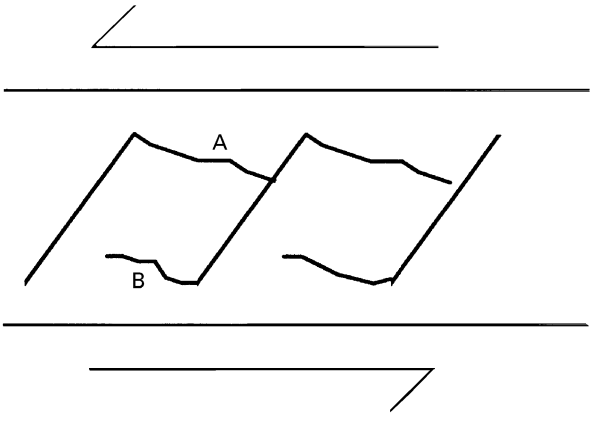

Figure 11 Crack A connecting between microcracks does not fully relieve the matrix stress between these microcracks as crack B can still be induced after crack A is fully developed.

2.4. Composite G_{IIC} in relation to controlling resin material variables

The macroscopically measured G_{IIC} (composite) using the ENF specimens has the form of [6]

$$G_{IIC} = \frac{9P^2a^2}{16B^2E_L h^3} \tag{29}$$

Equation 27 can also be rearranged into

$$\left(\frac{Pa}{Bh(E_L h)^{1/2}}\right) \propto \tau_c (t^{1+m}/GS^m)^{1/2} \tag{30}$$

Comparing Equations 29 and 30, it is obvious that

$$G_{IIC} \propto \tau_c^2 t^{1+m}/GS^m \tag{31}$$

By substituting Equations 24 and 28 into Equation 31, G_{IIC} becomes

$$G_{IIC} \propto G_{IC} t^{1+m} (\tau_y^2/GG_{IC}t)^{(1+m)/2} \tag{32}$$

or

$$G_{IIC} \propto G_{IC}^{(1-m)/2} (\tau_y^2/G)^{(1+m)/2} t^{(1+m)/2} \tag{33}$$

Equation 28 stands for the parametric dependence of laminate G_{IIC} on resin properties. It can be seen from this equation that G_{IIC} is not simply controlled by the resin G_{IC} but also by other resin variables that govern the failure process involved. As previously discussed, from the general nature of the G^* versus (S/t) curve in Fig. 9, $0 < m < 1$ is expected. For composite systems with a similar resin content, the G_{IIC} of Equation 33 can be reduced to the following form for comparison purposes:

$$G_{IIC} \propto G_{IC}^{(1-m)/2} (\tau_y^2/G)^{(1+m)/2} \quad (0 < m < 1) \tag{34}$$

3. Comparison of theory and experimental results

The failure mechanisms described in terms of Equations 33 and 34 can be applied to interpret the experimental results of laminate G_{IIC} and neat resin G_{IC}, τ_y and G of the Ciba epoxy/carbon fibre composite systems R914/T500, R922/T500 and R6376/T500 where T500 are carbon fibres made by Amoco. These resin and laminate properties are given in Table 1. The laminate G_{IIC} values were measured by using the ENF technique [6] and the resin G_{IC} values by the three-point bend method recommended by ASTM [15]. Resin τ_y and G values were obtained from yield strength σ_y and modulus E measured from neat resin compression tests as described in reference [18] by using the relations $\tau_y = \sigma_y/(3)^{1/2}$ and $G = E/2(1 + v)$ where v is Poisson's ratio (~ 0.3). It can be seen from Table I that laminate G_{IIC} values are not proportional to resin G_{IC}. The R922 system, an untoughened epoxy system, has a lower resin G_{IC} but a higher laminate G_{IIC} than the R914 system that was somewhat toughened.

To demonstrate the importance of different parameters in controlling laminate G_{IIC}, the $G_{IC}^{(1-m)/2} (\tau_y^2/G)^{(1+m)/2}$ term from Equation 34 is calculated for $m = 0.3, 0.5, 0.7$ and is given in Table 1. It can be seen that the $G_{IC}^{(1-m)/2} (\tau_y^2/G)^{(1+m)/2}$ values generally follow the trend of laminate G_{IIC} for the systems studied here (especially for $m < 0.5$). The resin G_{IC} contribution to G_{IIC} is obviously not dominant since the mode II delamination failure is not merely straight mode I for the matrix resin at the microscopic level.

The obvious dependence of laminate G_{IIC} on resin G_{IC} and (τ_y^2/G), even in the simplified form of Equation 34, is quite plausible to explain many other G_{IIC} related fracture phenomena. For example, the lack of loading rate and temperature sensitivity of G_{IIC} [5] can be attributed to the two controlling resin parameters usually following opposite trends when test conditions are varied. For instance, as the temperature increases (or loading rate decreases) the resin G_{IC} would increase and the (τ_y^2/G) term likely decreases thereby the two terms counteract each other to produce the $G_{IC}^{(1-m)/2} (\tau_y^2/G)^{(1+m)/2}$ term (Equation 34) and thus a laminate G_{IIC} that is rather insensitive to temperature changes.

It should be pointed out that the analysis as modelled assumes limited resin plastic deformation so that the microcracking process is not suppressed by the yielding mechanism. Plastic deformation may eventually be induced after the microcracks reach the saturation spaces S. However, such plastic deformation is assumed to be negligible and not to affect the described microcrack coalescence process. Indeed, this is a reasonable assumption since the hackle marking did not have an observable change of shape after the fractured specimens were heated above their T_g's in this and other reported studies [1].

Such observations, however, may be limited to thermoset-based systems. For thermoplastic composites, the resin G_{IC} is much higher and τ_y much lower than those of the thermoset counterpart. The microcrack spacing $S \propto (tG_{IC}G/\tau_y^2)^{1/2}$ (Equation 24) of thermoplastic resins in the composites will be much larger than that of thermosets. Large amounts of plastic deformation may be more dominant than microcrack coalescence which for thermoplastic systems will be more difficult to induce because of larger S. It is even possible that matrix plastic deformation can

TABLE I Resin and laminate parameters related to mode II delamination

		Resin properties			$G_{IC}^{(1-m)/2} (\tau_y^2/G)^{(1+m)/2}$		
Resin system	Laminate G_{IIC} (kJ m^{-2})	G_{IC} (kJ m^{-2})	τ_y (MPa)	G (MPa)	$m = 0.3$	$m = 0.5$	$m = 0.7$
R914	0.50	0.11	90	1570	1.34	1.97	2.90
R922	0.60	0.08	118	1640	1.65	2.65	4.22
R6376	0.70	0.37	103	1580	2.43	3.25	4.35

completely suppress its competing mechanism of microcracking when the matrix yield strength is relatively low. Such a matrix yielding dominated mechanism was reflected in the previously reported study [5] on a carbon fibre/thermoplastic composite system AS4/PEEK which showed mode II delamination fracture surfaces having extensive matrix deformation without microcracking. G_{IIC} of this system also decreased with increasing temperature, following the generally known trend of resin τ_y (instead of G_{IC}) as a function of temperature for polymers.

4. Conclusions

The failure process of mode II delamination fracture was studied on the basis of the microscopic matrix failure modes (microcracks and hackles) as well as fracture mechanics principles. The crack tip matrix stresses leading to delamination were analysed by examination of an adhesive bond with a crack analogous to a delamination crack in the resin layer of a composite. Such crack tip stresses induce matrix microcracks involving two major events: (a) single microcrack initiation and (b) development of multiple microcracks with regular spacing. The microcrack initiation shear stress τ^* was found, by use of fracture mechanics, to be related to certain resin properties (shear modulus G and mode I fracture toughness G_{IC}) and microcrack length of the order of the resin layer thickness t (related to resin content). The more or less regular microcrack spacing S deduced from shear lag considerations can be related to resin properties G_{IC}, G, τ_y (resin yield strength) and t. The multiple microcracks reduce the effective resin modulus and strongly affect the subsequent microcrack coalescence process. As a result of the detailed analysis of the failure process, mode II laminate fracture toughness G_{IIC} can be quantitatively expressed as a function of resin G_{IC} and (τ_y^2/G). The failure process modelled was used to interpret the mode II delamination behaviour of several carbon/epoxy systems. This study reveals the critical importance of resin fracture (G_{IC} related) and deformation (yielding) mechanisms in controlling mode II delamination resistance of laminated composites.

References

1. M.F. HIBBS and W. L. BRADLEY, "Correlations Between Micromechanical Failure Processes and the Delamination Toughness of Graphite/Epoxy Systems", ASTP-948, (American Society for Testing and Materials, Philadelphia PA, 1987) p. 68.
2. L. ACRAN, M. ACRAN, and I. M. DANIEL, "SEM Fractography of Pure and Mixed Mode Interlaminar Fractures in Graphite/Epoxy Composites", ASTM STP-948, (American Society for Testing and Materials, Philadelphia PA, 1987) pp. 41–67.
3. B. W. SMITH and R. A. GROVE, "Determination of Crack Propagation Directions in Graphite/Epoxy Structures", ASTM STP-948 (American Society for Testing and Materials, Philadelphia PA, 1987) pp. 154–173.
4. A. J. RUSSEL, *Polymer Compos* **8** (1987) 342.
5. P. DAVIES and F. X. de CHARENTENAY, in Proceedings of 6th International Conference on Composite Materials (ICCM-VI), London, July 20–24, 1987, (Elsevier, London, 1987) p. 3.284.
6. A. J. RUSSEL and K. N. STREET, in "Moisture and Temperature Effect on the Mixed Mode Delamination Fracture of Unidirectional Graphite/Epoxy, edited by W. S. Johnson, ASTM STP 876, (American Society for Testing and Materials, Philadelphia PA, 1985) pp. 349–370.
7. G. B. MURRI and T. K. O'BRIEN, in Proceedings of the 26th AIAA/ASME/AHS Conferences on Structures, Structural Dynamics and Materials, Orlando, FL, April 15–17, 1987 (American Institute of Aeronautics and Astronautics (AIAA), New York, 1985) p. 172.
8. L. A. CARLSSON, J. W. GILLESPIE and B. R. TRETHEWEY, *J. Reinf. Plastics* **5** (1987) 170.
9. S. M. LEE, *J. Mater. Sci.* **19** (1984) 2278.
10. *Idem*, *Polm. Engng. Sci.* **27** (1987) 77.
11. *Idem*, "Fracture Mechanism of Delamination Fracture", edited by J. D. Whitcomb, ASTM STP-972 (American Society for Testing and Materials, Philadelphia PA, 1988) pp. 356–365.
12. A. PARVIZI, K. W. GARRETT and J. E. BAILEY, *J. Mater. Sci.* **13** (1978) 195.
13. A. PARVIZI and J. E. BAILEY, *ibid.* **13** (1978) 2131.
14. J. E. BAILEY, P. T. CURTIS and A. PARVIZI, *Proc. Roy. Soc. London* **A 366** (1979) 599.
15. D. BROEK, "Elementary Engineering Fracture Mechanics", (Martinus Nijhoff Publishers, The Hague, 1983).
16. H.-J. SUE, R. E. JONES and E. I. GARCIA-MEITEN, *J. Mater. Sci.* **28** (1993) 6381.
17. E. I. GARCIA-MEITIN and H.-J. SUE, *Polym. Compos.* **15** (1994) 165.
18. S. LEE and R. SCHILE, *J. Mater. Sci.* **17** (1982) 2066.

Received 14 August 1995
and accepted 13 June 1996